INL/CON-23-72763-Revision-0

Additively Manufactured Strain Sensing for Nuclear Reactor Applications

July 2023

Timothy Le Phero, Kiyo T Fujimoto, Amey Rajendra Khanolkar, Michael D McMurtrey, Benjamin Johnson, David Estrada, Brian Jaques, Kaelee Novich

Changing the World's Energy Future

INL is a U.S. Department of Energy National Laboratory operated by Battelle Energy Alliance, LLC

INL/CON-23-72763-Revision-0

Additively Manufactured Strain Sensing for Nuclear Reactor Applications

Timothy Le Phero, Kiyo T Fujimoto, Amey Rajendra Khanolkar, Michael D McMurtrey, Benjamin Johnson, David Estrada, Brian Jaques, Kaelee Novich

July 2023

Idaho National Laboratory
Idaho Falls, Idaho 83415

http://www.inl.gov

Prepared for the
U.S. Department of Energy
Under DOE Idaho Operations Office
Contract DE-AC07-05ID14517

Additively Manufactured Strain Sensing for Nuclear Reactor Applications

Timothy L. Phero[1,3,4] and Kaelee A. Novich[1,3], Kiyo T. Fujimoto[4], Amey R. Khanolkar[4], Benjamin C. Johnson[2], Michael D. McMurtrey[4], David Estrada[1,3,4], Brian J. Jaques[1,3,*]

[1]Micron School of Materials Science and Engineering, Boise State University, Boise, ID
[2]Department of Electrical and Computer Engineering, Boise State University, Boise, ID
[3]Center for Advanced Energy Studies, Idaho Falls, ID
[4]Idaho National Laboratory, Idaho Falls, ID

ABSTRACT

Real-time monitoring of materials in harsh environments is a crucial technique towards reducing innovation time in nuclear systems. The successful measurement of real time, in-situ strain measurements during nuclear reactor operation requires innovative sensing solutions, including novel sensing strategies as well as advanced sensor design, manufacturing, and materials selection. In this paper, we will discuss two primary strategies for in-situ strain measurement strategies: additively manufactured (AM) capacitive strain gauges (CSGs) and digital image correlation (DIC).

Current commercial strain gauges have limited applications in reactors due to the harsh operating conditions and non-trivial attachment strategies (i.e., welding, epoxy-adhesive) that can affect both the sensing performance and the underlying substrate under testing. AM CSGs are a viable solution as they have a low profile, low hysteresis, and wireless sensing integration capabilities that will enhance nuclear sensing technologies. In this work, the mechanical and thermal performance of the AM CSGs were tested up to 300 °C using ASTM standardized testing procedures to simulate the temperatures found in existing light water reactors. The AM CSGs had a similar performance across multiple samples which correlates to analytical models. This work leads towards the development of CSGs designed for higher temperatures and additional environmental factors found in Generation-IV reactors.

Non-contact sensors, such as DIC, offer a less destructive way to measure deformation of materials when compared to alternative methods of in-situ strain determination, such as weldable strain gauges. However, DIC requires high contrast surfaces, which often relies on the implementation of artificial patterns. Using traditional splatter techniques to fabricate these patterns have limitations, including poor surface adhesion and reproducibility. In this work, AM fabrication techniques were implemented to avoid such limitations. Accordingly, aerosol jet printing (AJP) was used to print small scale periodic patterns of silver on stainless steel and aluminum tensile specimens. DIC was employed to monitor strain (up to 1100 με) during temperature cycling from 23-600 °C. The results validated the use of AJP to better control pattern parameters for small fields of view applications at high temperatures.

Keywords: Additive Manufacture, strain, sensing, digital image correlation

1. INTRODUCTION

The non-intrusive interrogation of strain sensors in nuclear-related environments, such as test reactors that are used for irradiation studies in materials and fuels, enables for the measurement of crucial mechanical phenomena. Current strain sensors, including resistance-based strain gauge (RSG) technologies, are both well established and commercially available; however, they present limitations in terms of test reactor experiment conditions, especially in areas where physical space is a challenge. The successful deployment of reliable strain sensing methodologies in reactor conditions stands to benefit from improved sensor design and manufacturing that allow for its application within the wide nuclear test space (i.e., environment, sample geometry, materials compatibility). Two in-situ strain sensing strategies being investigated in this work are capacitive strain gauges (CSG) and digital image correlation (DIC). CSGs and DIC harmoniously work together to validate material deformation and provides a wider strain sensing selection, which will be more accommodating to current and future test rig setups.

Interdigitated electrode (IDE) CSGs are of interest since they have been shown to have enhanced performance in high strain conditions when compared to commercially available high-elongation RSGs [1]. The IDE design enables for a low-profile CSG with multiple in-plane electrodes that are parallel to the substrate, which have been shown to have high strain sensitivity and low hysteresis [2, 3]. In addition, the capacitive sensing mechanism of CSGs have shown to be better suited for long-term static measurements in harsh environments due to its low environmental sensitivity to high-temperature degradation effects (e.g., oxidation) that affect the electrical performance of RSGs [1, 4-6]. The low-profile nature, high temperature compatibility, and suitability for wireless signal transmission [2, 7] make the IDE CSG a promising design and sensing mechanism for strain gauges in harsh environments.

In addition to CSGs, DIC provides a complementary non-contact, optical method of measuring strain, which may prove to be useful in areas where it is difficult to implement direct contact sensors. DIC relies on a reference image being taken before testing conditions commence and then will compare the reference image to the image that are taken during testing through image analysis. This process typically uses Gauss-Newton or Newton-Raphson algorithms. DIC has become a popular strain measuring technique due to its cost effectiveness and relatively simple execution in setup [8-10]. There are only three primary parts to DIC: pattern fabrication, experimental setup, and image-to-strain computation. Due to the harsh environment of a nuclear reactor, DIC will be challenging to implement. However, the use of DIC will be instrumental to in-situ test reactor experiments if successfully demonstrated. Some of these challenges include line of sight, lighting, image resolution, and pattern sustainability. The following work focuses on improving DIC patterns for temperatures ranging from 23-600 °C since test reactor experiments operate within such temperatures [11, 12].

CSGs and DIC are both viable sensor techniques that are complementary to each other and benefit nuclear sensing applications. The current inability to purchase CSGs or produce repeatable DIC patterns that withstand test reactor environments can be solved through direct write additive manufacturing (AM) technologies. For CSGs, AM capabilities improve fabrication time for IDE CSGs and offset the geometry and materials limitations of traditional fabrication techniques. Accordingly, AM can also be used to create repeatable, high contrast DIC patterns. DIC patterns typically created using a splattering technique are limited by operator dependency, lack of reproducibility, and variation in speckle size and distribution. In recent years, AM has demonstrated the ability to fabricate sensors and patterns that can overcome the high temperature environments (i.e., above 300 °C conditions; [4]) and non-planar, geometric challenges (i.e., cylindrical geometries; [13]) that are commonly found in nuclear reactors. In addition to allowing the deposition of up to a sub-micron feature size, the flexibility of AM allows for it to be compatible with tailorable, nuclear-relevant ink materials [14] making it an ideal tool for the rapid prototyping of both CSGs and DIC patterns for in-pile applications. In this work, the performance of AM sensing techniques were tested up to 300 °C and 600 °C for the CSG and DIC patterns, respectively.

2. EXPERIMENTAL METHODS

An AM technique called aerosol jet printing (Aerosol Jet Series 200, Optomec) with silver nanoparticle ink was used to fabricate both the DIC pattern and IDE CSG on stainless steel 316L (SS316L) and/or an aluminum 6061 (Al6061) tensile specimens due to its use in nuclear research reactors[15]. Prior to fabrication, the tensile specimens were prepared by grinding the printing surface with 180 grit silicon carbide paper to level and remove surface oxidation. The substrates were then rinsed with both acetone and de-ionized water to degrease and clean the surface immediately prior to sensor application.

For testing, a mechanical test fixture (MTS Series 793) was used to perform tensile experiments (Fig. 1) of both the CSG and DIC tests. A high temperature extensometer (MTS Model 632.53E-11) was used to validate the strain results. For mechanical testing at temperatures above ambient conditions, a two-zone furnace (MTS Series 793) was attached to the mechanical test fixture. The hydraulic grips (MTS 647 Hydraulic Wedge Grips) fitted on the mechanical test fixture are only rated to 177 °C and was therefore shielded from extreme temperatures by incorporating cooling lines into the wedges. In addition, the wedges were coated with Perma-Silk lubricant (Perma-Silk RAC, Everlube Products) as recommended by the Series 647 Hydraulic Wedge Grips Reference Manual [16]. Between the furnace and the hydraulic grip, a ceramic fiber insulation with a temperature rating up to 1371 °C was inserted into the system. Fans were also added to the setup to regulate airflow and to reduce the temperature gradient from the top and bottom heat elements in the furnace. Two thermocouples were inserted into the heat zone near the top and bottom of the gauge length region of the tensile specimen and were monitored using a temperature controller (MTS Model 409.83). The following sections will provide further information on the preparation of the CSG and DIC samples.

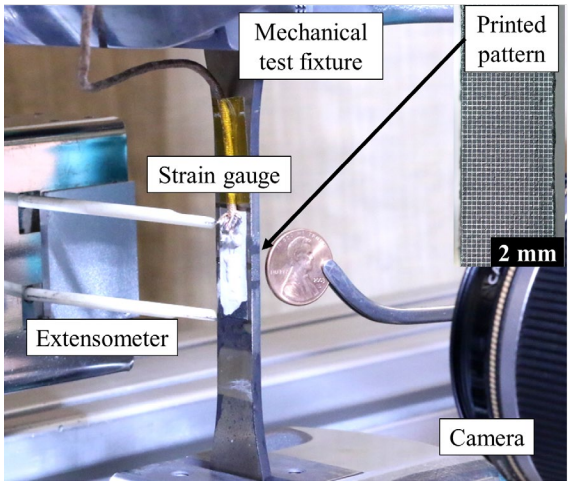

Figure 1. An example experimental setup of a strain gauge and digital image correlation (DIC) pattern placement for room temperature tensile strain tests. Each specimen was placed in the mechanical test fixture and the edge of the camera lens was brought 60 mm away from the DIC pattern.

2.1. CSG Preparation

The multi-layered packaging of the CSG using aerosol jet printing (AJP) is comprised of the substrate, an insulative layer, and the conductive electronic sensor. In a previous work, it was found that polyimide served as a viable insulation layer since it was commercially available, electrically insulative, sufficiently elastic, and stable at elevated temperature up to 400 °C. After preparing the surface of the tensile

specimen, a 25 μm thick high temperature polyimide tape was adhered to the gauge length of the tensile specimen. To ensure proper adhesion and minimal entrapment of air of the polyimide tape to the substrate, a hand operated pressure roller was used to apply even pressure across the surface of the tape. The overall dimension of the IDE CSG (Fig. 2) was designed to maximize the sensing performance and overall gauge region of the tensile specimen.

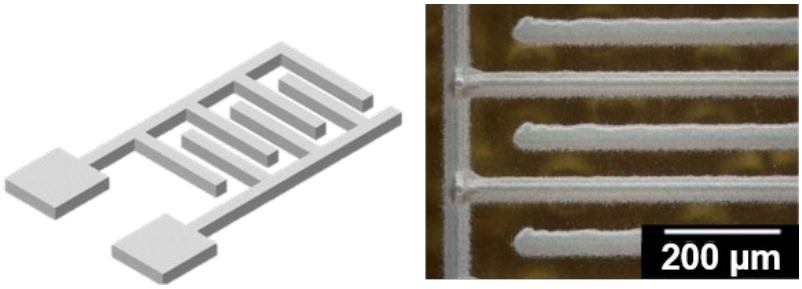

Figure 2. Schematic and representative print of the interdigitated electrode design used for the capacitive strain gauge.

2.2. DIC Preparation

2.2.1. Pattern fabrication

Due to the geometry of the mechanical test fixture that was used for experiments, DIC patterns (6 mm by 3 mm) were fabricated on the thin sides (3 mm wide) of the SS316L and Al6061 tensile specimen. After preparing the sides of the specimens, they were spray-painted (black silica ceramic coating, Helix Racing Products) to achieve a background for the printed pattern to be deposited on. For the spray-painted DIC patterns, white spray paint was applied after this step to create a random distribution of speckles (Fig. 3). AJP can be used to make any pattern that the user desires and periodic patterns were chosen for the experiments in this work as shown in Fig. 3. After curing the silver nanoparticle ink, the printed pattern provided a bright white contrast to the black, spray-painted background.

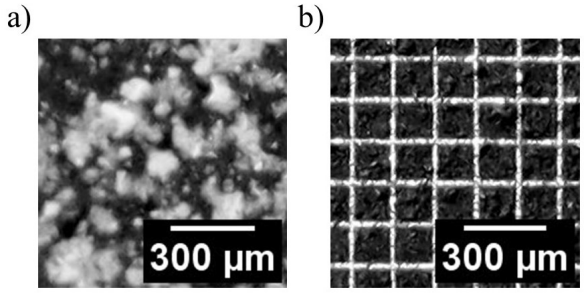

Figure 3. DIC patterns prepared using a) spray-painting and b) printing techniques. The printed pattern was composed of vertical and horizontal lines with 150 μm pitch. All patterns were 6 mm by 3 mm.

DIC patterns were validated using a commercially available resistive strain gauge (HFH-12-250-ZHW, Hitec Products, 120 Ω wire), which was placed at the face of the gauge length region of the SS316L and Al6061 specimens. Strain gauges were attached using a ceramic cement (NCC-3 and HG-1, Hitec Products) and were used following a similar process outlined by Phero et al. [17].

2.2.2. Image analysis

Images taken during experiments were prepared for DIC computational analysis by using ImageJ to convert images to 8-bit [18]. The images were also sized to the region of interest, which had a resolution of 1548 x 810 pixels. Ncorr (version 1.2), an open-source software for DIC, was used to compute strain values from the images. The software utilizes an inverse compositional Gauss-Newton to determine displacement fields with the aid of a Hessian matrix using subset-based matching. Subsets are small areas chosen on the image to track displacement from the reference image. The size, otherwise known as subset radius, and spacing of subsets are controlled by the user. While the images were being processed in Ncorr, the subset radius was selected as 44 pixels with a spacing of 3 pixels. The region of interest was considered to be the entire pattern, which was 6 mm by 3 mm. Ncorr typically required 10 to 19 iterations before computing displacement and strain fields.

2.2.3. Mechanical Setup

For the tests in this study, specimens underwent cyclic tensile loads following ASTM E251 - 92 and ASTM E83 - 16 as suggested by ASTM E2208 - 02 , which serves as guide for non-contact optical strain sensors. All images were taken using a Canon EOS 90D. The camera was fitted with a 60 mm macro lens to improve the resolution of the small field of view. The lens was manually focused on the pattern before each test. Since the DIC setup followed a 2D set up, the camera lens was placed perpendicular to the DIC pattern as shown in Fig. 1. For SS316L samples, images were taken every 20 seconds during experiments at room temperature to 600 °C. Al6061 samples were only tested at room temperature and images were taken every 15 seconds. DIC patterns were illuminated with white light at 2000 lumens. There were a total of four cyclic tensile tests with each DIC pattern type at 23 °C, 100 °C, 200 °C, 300 °C, and 600 °C. The camera was brought back by 120 mm to fit into the setup when the furnace was closed during testing at elevated temperatures.

3. RESULTS

3.1. CSG Results

Fig. 4 shows the mechanical testing results for the CSGs and compares them to analytical models [3, 19]. To quantify the sensitivity of the CSGs, the gauge factor of the strain sensor is calculated by using:

$$Gauge\ Factor\ = \frac{\Delta C/C_o}{\varepsilon}, \tag{1}$$

where C is capacitance and ε is mechanical strain. Between room temperature and 300 °C, the gauge factor was found to be between 0.85 and 0.91 (Table I). When compared to a similar CSG printed on Al6061 substrate [17], the CSG printed on SS316L had a more consistent gauge factor than the one printed on Al6061. Furthermore, on SS316L, the strain gauge was able to be tested up to 1000 με at the higher 200 °C and 300 °C temperatures, unlike the trends observed for Al6061 by Phero et al. [17]. This further suggests that the deviations from the Al6061 trends reflect a drastic degradation in the mechanical properties of the substrate, and not a problem with the IDE CSG system itself.

The sensitivity of the CSG also continued to match well with analytical model from Kim, et al. [3] and deviated from the model from Hu, et al [19]. Work from Kim, et al. shows that the sensing performance

of the IDE CSG can be calculated on an equation based on only strain (ε) and the Poisson's ratio (υ) of the substrate, according to (Eq. 2):

$$\frac{\Delta C}{C_o} = \frac{(1-\upsilon\varepsilon)\cdot(1-\upsilon\varepsilon)}{(1+\varepsilon)} - 1 \quad (2)$$

Eq. (2) shows that an increase in Poisson's ratio of the underlying substrate increases the CSG's sensitivity to strain. The Poisson's ratio of SS316L and Al6061 are 0.27 and 0.33 at room temperature, respectively. When compared to the CSG on Al6061 (Table I), the lower gauge factor of the CSG on SS316L make sense due to the lower Poisson's ratio of the substrate material.

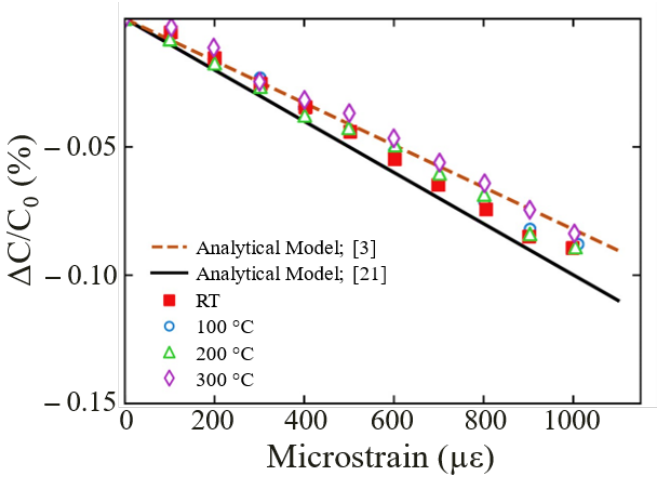

Figure 4. Tensile strain output of a capacitive strain gauge printed onto a SS316 substrate tested at temperatures ranging from RT to 300 °C. Despite the substrate change, the output closely matches the results from the analytical models [3, 19] previously discussed in Phero et al. [17].

Table I. Summary of the initial readings and gauge factor (GF) of CSGs tested from room temperature to 300 °C. The gauge factor was calculated using the experimental results shown in Fig. 4

Reference	Substrate	Initial Capacitance (pF)	GF at room temperature	GF at 100 °C	GF at 200 °C	GF at 300 °C
[17]	Al6061	12.16	0.97	1.08	1.87	1.68
This paper	SS316L	12.58	0.91	0.90	0.89	0.85

3.2. DIC Results

Tensile tests were performed at 23 °C, 100 °C, 200 °C, 300 °C, and 600 °C with samples having printed and spray-painted DIC patterns. The statistical significance and coefficient of determination was found to investigate the error between the strain calculated by the DIC patterns and the strain measured by the extensometer.

3.2.1. Mechanical loading, 23-600 °C

Images of the DIC patterns were taken during tensile tests with Al6061 and SS316L samples at room temperature. The strain calculated from DIC was compared to the strain measured by the extensometer and strain gauges used during experiments. The extensometer was set as the reference since it was previously calibrated following the ASTM E83 Class B1 standard [20] and the strain gauges were a secondary validation method to measuring the strain using DIC. For tests with both materials, all strain measurements correlated well with each other as shown in Fig. 5.

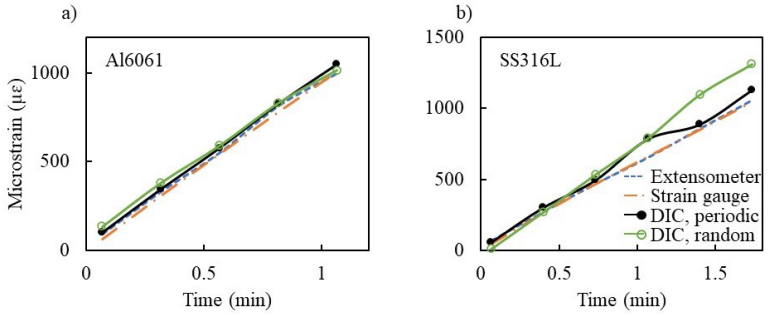

Figure 5. Tensile test results for Al6061 and SS316L specimens at room temperature. Strain results calculated from the DIC patterns matched well with the strain measured by the extensometer and commercial resistive strain gauges.

For experiments above room temperature, the tensile load was decreased to keep all SS316L samples within the elastic region. Cyclic loading was performed at 100 °C, 200 °C, 300 °C, and 600 °C (Fig. 6). Once the desired temperature was reached, tensile tests were not performed until the material had reach thermal equilibrium. Thermal expansion of the material was determined by the extensometer, which was monitored in real time. All strain values calculated by DIC matched well with the strain measured by the extensometer. More specifically, the periodic pattern resulted in strain values that were either similar or more accurate to the data correlating to the spray-painted (random) pattern.

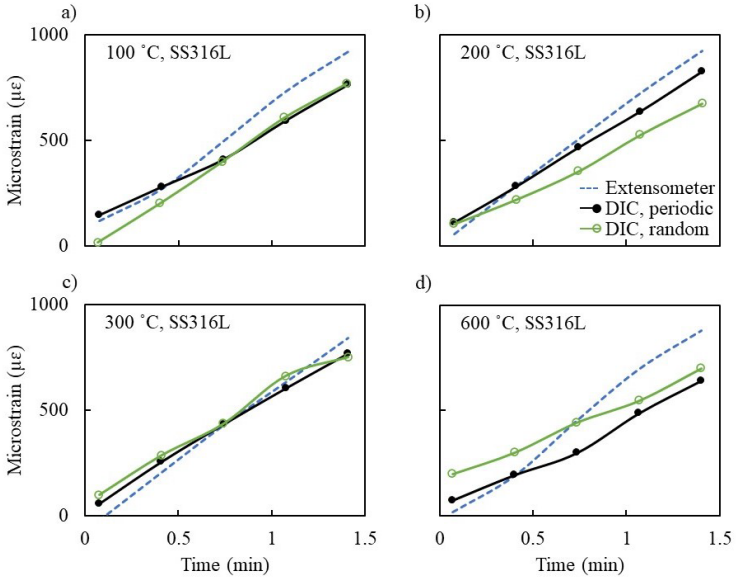

Figure 6. Tensile loading was performed on SS316L specimens with DIC patterns at 100 °C, 200 °C, 300 °C, and 600 °C. The loading was reduced to below 1000 microstrain to stay within the elastic region of the samples.

3.2.2. Error analysis

The statistical significance and coefficient of determination was determined by comparing the strain data tabulated from the DIC patterns to the strain results from the extensometer (Table II). Strain results from both DIC patterns accurately correlated to the data from the extensometer. All P-values were greater than 0.05 and indicated that there was no statistical significance between the two sets of data. Since the data was assumed to be linear based on the experiments performed, the strain results between the DIC patterns and extensometer were plotted against each other and the coefficient of determination was found. Accordingly, the coefficient of determination was 0.98 or higher for all experiments.

Table II. Statistical significance (P-value) and coefficient of determination (R^2) between DIC patterns and extensometer

Sample	Temperature (°C)	DIC Type	R^2	P-value
Al6061	23	Periodic	0.995	0.815
		Random	0.998	0.866
SS316L	23	Periodic	0.988	0.801
		Random	0.996	0.482
	100	Periodic	0.995	0.614
		Random	0.994	0.869
	200	Periodic	0.999	0.809
		Random	0.997	0.720
	300	Periodic	0.999	0.996
		Random	0.993	0.485
	600	Periodic	0.985	0.535
		Random	0.996	0.788

4. CONCLUSION

With further development, AM CSGs could serve to alleviate challenges arising from size constraints, material restrictions, and invasive integration strategies. In its current state, printed CSGs are not ready for nuclear applications; however, this work demonstrates that AM is a viable manufacturing strategy for fabricating functional strain gauges for measuring mechanical strain in environmental temperatures of up to 300 °C. The work demonstrates that the CSG had a stable gauge factor of about 0.90 up to 300 °C maintains its correlation to analytical models despite a change in substrate from Al6061 to SS316L. Future efforts are exploring the fabrication of IDE CSGs made solely of metal and ceramic constituent layers less susceptible to damage and degradation. This extends the potential applications of AM CSG to higher temperature applications (i.e., up to 500 °C).

Using AM techniques, such as AJP, to build DIC patterns is a favorable method to measuring deformation in extreme environments. Printed DIC patterns were used on Al6061 and SS316L samples at 23 °C, 100 °C, 200 °C, 300 °C, and 600 °C. The results calculated from the pattern with periodicity was compared to strain that was found from a traditional spray-painted pattern. All strain values computed using DIC were validated using a high temperature extensometer at all temperature and resistive strain gauges at room temperature. The results from the DIC patterns matched with the strain measured by the

extensometer and resistive strain gauges with low margins of error based on the statistical significance and coefficient of determination. Since ASTM E2208 – 02 standard does not provide classifications for allowable error associated to DIC setups [21], the error from the DIC calculated strain results was compared to the categorization of extensometers in ASTM E83 - 16 [20]. Class B1 extensometers are able to have a fixed error of ±100 microstrain and class C extensometers have a fix error of ±1000 microstrain. AM DIC patterns would fit closer to a class B1 extensometer and would be suitable for nuclear application from the temperatures that were observed in this study. Additionally, AM capabilities offered a fabrication process that was repeatable and would be adequate for small fields of view, which is likely desirable when implementing DIC into nuclear reactors.

ACKNOWLEDGMENTS

This work was prepared as an account of work sponsored by the U.S. Department of Energy, Office of Nuclear Energy Advanced Sensors and Instrumentation program under DOE Contract DE- AC07-05ID14517. Neither the U.S. Government nor any agency thereof, nor any of their employees, makes any warranty, expressed or implied, or assumes any legal liability or responsibility for the accuracy, completeness, or usefulness, of any information, apparatus, product, or process disclosed, or represents that its use would not infringe privately owned rights. References herein to any specific commercial product, process, or service by trade name, trademark, manufacturer, or otherwise, does not necessarily constitute or imply its endorsement, recommendation, or favoring by the U.S. Government or any agency thereof. The views and opinions of authors expressed herein do not necessarily state or reflect those of the U.S. Government or any agency thereof. Additionally, this material is based upon work supported under a University Nuclear Leadership Program Graduate Fellowship through the Department of Energy, Office of Nuclear Energy.

REFERENCES

1. K. T. Fujimoto, J. K. Watkins, T. Phero, D. Litteken, K. Tsai, T. Bingham, K. L. Ranganatha, B. C. Johnson, Z. Deng, and B. Jaques, “Aerosol jet printed capacitive strain gauge for soft structural materials,” *npj Flexible Electronics,* **vol. 4**, no. 1, pp. 1-9, 2020.
2. H. Nesser, J. Grisolia, T. Alnasser, B. Viallet, and L. Ressier, “Towards wireless highly sensitive capacitive strain sensors based on gold colloidal nanoparticles,” *Nanoscale,* **vol. 10**, no. 22, pp. 10479-10487, Jun, 2018.
3. S.-R. Kim, J.-H. Kim, and J.-W. Park, “Wearable and transparent capacitive strain sensor with high sensitivity based on patterned Ag nanowire networks,” *ACS applied materials & interfaces,* **vol. 9**, no. 31, pp. 26407-26416, 2017.
4. M. T. Rahman, R. Moser, H. M. Zbib, C. V. Ramana, and R. Panat, “3D printed high performance strain sensors for high temperature applications,” *Journal of Applied Physics,* **vol. 123**, no. 2, pp. 1-12, Jan 14, 2018.
5. ASTM, “E1319 - 98: Standard Guide for High-Temperature Static Strain,” *ASTM*, pp. 971-981, 2014.
6. B. Noltingk, D. McLachlan, C. Owen, and P. O'neill, "High-stability capacitance strain gauge for use at extreme temperatures." pp. 897-903.
7. K. L. Ranganatha, K. Novich, T. Phero, K. T. Fujimoto, D. Litteken, D. Estrada, B. J. Jaques, and B. C. Johnson, "A Wireless, Multi-Channel Printed Capacitive Strain Gauge System for Structural Health Monitoring." pp. 1-4.
8. B. Pan, “Digital image correlation for surface deformation measurement: historical developments, recent advances and future goals,” *Measurement Science and Technology,* **vol. 29**, no. 8, pp. 082001, 2018/06/28, 2018.

9. Y. L. Dong, and B. Pan, “A Review of Speckle Pattern Fabrication and Assessment for Digital Image Correlation,” *Experimental Mechanics,* **vol. 57**, no. 8, pp. 1161-1181, 2017/10/01, 2017.
10. G. M. Hassan, “Deformation measurement in the presence of discontinuities with digital image correlation: A review,” *Optics and Lasers in Engineering,* **vol. 137**, pp. 106394, 2021/02/01/, 2021.
11. A. J. Palmer, B. C. Hong, D. J. Stites, and F. W. Ingram, “Installation of the Irradiation Test Vehicle in the Advanced Test Reactor,” in Conference: Global '99, Jackson, WY, 08/29/99 - 09/03/99, United States, 1999, pp. Medium: ED; Size: 993 Kilobytes.
12. *Research Reactors*, World Nuclear Association, 2021.
13. S. Vella, C. Smithson, K. Halfyard, E. Shen, and M. Chretien, “Integrated capacitive sensor devices aerosol jet printed on 3D objects,” *Flexible and Printed Electronics,* **vol. 4**, no. 4, pp. 1-16, Dec, 2019.
14. K. T. Fujimoto, L. A. Hone, K. D. Manning, R. D. Seifert, K. L. Davis, J. N. Milloway, R. S. Skifton, Y. Wu, M. Wilding, and D. Estrada, “Additive Manufacturing of Miniaturized Peak Temperature Monitors for In-Pile Applications,” *Sensors,* **vol. 21**, no. 22, pp. 7688, 2021.
15. J. D. Tucker, Y. R. Wei, W. R. Marcum, P. V. Murkute, B. J. Gibbons, and O. B. Isgor, “Quantifying Oxide Layer Growth at Low Pressures and Temperatures for Aluminum Alloy 6061,” *Metallurgical and Materials Transactions a-Physical Metallurgy and Materials Science,* **vol. 50a**, no. 7, pp. 3388-3398, Jul, 2019.
16. "Series 647 Hydraulic Wedge Grips Reference Manual," MTS Systems: , 2013.
17. T. L. Phero, K. A. Novich, B. C. Johnson, M. D. McMurtrey, D. Estrada, and B. J. Jaques, “Additively manufactured strain sensors for in-pile applications,” *Sensors and Actuators A: Physical*, pp. 113691, 2022.
18. C. A. Schneider, W. S. Rasband, and K. W. Eliceiri, “NIH Image to ImageJ: 25 years of image analysis,” *Nature Methods,* **vol. 9**, no. 7, pp. 671-675, 2012.
19. C.-F. Hu, J.-Y. Wang, Y.-C. Liu, M.-H. Tsai, and W. Fang, “Development of 3D carbon nanotube interdigitated finger electrodes on polymer substrate for flexible capacitive sensor application,” *Nanotechnology,* **vol. 24**, no. 44, pp. 444006, 2013.
20. ASTM, "E83 - 16: Standard Practice for Verification and Classification of Extensometer Systems," 2017, pp. 264-77.
21. ASTM, "E2208 - 02: Standard Guide for Evaluating Non-Contacting Optical Strain Measurement Systems," 2018, pp. 1-7.